Paper No. 941547
An ASAE Meeting Presentation

PREDICTION OF SOIL STRESSES CAUSED BY TIRE INFLATION PRESSURES AND DYNAMIC LOADS

by

R. L. Raper, A.C. Bailey, E.C. Burt
Agricultural Engineers
USDA, ARS, National Soil Dynamics Laboratory
P.O. Box 3439, Auburn, AL 36831-3439 USA

C.E. Johnson
Professor
Agricultural Engineering Department
Auburn University, Auburn, AL 36849 USA

Written for presentation at the
1994 International Winter Meeting
sponsored by
AMERICAN SOCIETY OF AGRICULTURAL ENGINEERS

Atlanta Hilton and Towers
Atlanta, Georgia
December 13-16, 1994

Summary:

Peak soil-tire interface stresses were measured on the surface of a tire during a series of experiments examining dynamic load-inflation pressure combinations. Dynamic load and inflation pressure were both found to affect the peak soil-tire interface stresses on the lug of a tire. A finite element model then used these values to predict the stress distributions in the soil.

Keywords:

Finite element analysis, tire, axle load, soil compaction, soil-tire interface stresses

ASAE, 2950 Niles Rd., St. Joseph, MI 49085-9659 USA
Voice: 616.429.0300 FAX: 616.429.3852

INTRODUCTION

The process of soil compaction is complex, often difficult to understand, even with complicated modeling processes. Several researchers using the finite element method have attempted to model soil compaction using various soil stress-strain relationships. Hyperbolic stress-strain models for soil were used by Duncan and Chang (1970), Pollock et al. (1986), Chi and Kushwaha (1989), and Chi et al. (1993) to predict soil compaction. Other stress-strain relationships using mean normal stress (Raper and Erbach, 1990) and octahedral normal stress and octahedral shearing stress (Raper et al., 1994) have been used to predict soil behavior when soil was subjected to compacting forces.

One of the difficulties in predicting soil compaction has been measuring and applying complex surface loads to the model. These forces are rarely simple vertical point loads as modeled by Boussinesq (1885) or uniform loads as modeled by Frohlich (1934). Perumpral et al. (1971) and Pollock et al. (1986) assumed a circular uniform stress distribution across the surface to provide the input loads into their finite element models. The circular assumption for these papers was used for the loading because of the need to assume axisymmetric geometry for the soil. This two-dimensional problem required much less computational power than a true three-dimensional finite element model. Raper and Erbach (1990) also used axisymmetric geometry to model the soil compaction beneath a flat circular disk.

Another simplified modeling assumption that used a plane strain finite element model to predict soil compaction beneath a rigid wheel was used by (Raper et al., 1992). The rigid wheel was assumed to be infinitely wide and was similar to a roller. A true three-dimensional finite element model was constructed by Chi et al. (1993) to model the soil compaction beneath heavy liquid manure spreaders, Chi et al. (1993) assumed the loading to be rectangular with uniform pressure distribution.

The actual forces on the soil caused by tractive devices are often composed of both normal and tangential components that manipulate and compact the soil and vary over their width. A simplified approach to this complex surface loading has been to consider the effect of total load or axle load that assumes uniform vertical loading over a circular footprint. Taylor et al. (1980) used this term to compare two bias-ply tires that used the same inflation pressure, but different dynamic loads. One tire was an 18.4 x 38 10-ply bias and the other was a 30.5Lx32 10-ply bias. Each tire was operated at the same inflation pressure, 110 kPa, but at their respective rated dynamic loads: 23.3 kN and 40.5 kN. The results of this experiment showed that vertical soil pressures and soil bulk densities beneath the center of the tire are slightly larger for the larger tire. These differences are small, however, and this comparison was not the general focus of Taylor's paper.

Alabama Agricultural Experiment Station Journal No. 2-944942

This project was conducted as a part of USDA Regional Project S-252.

A major series of experiments was conducted throughout the world by researchers using the axle load concept (Hakansson, 1994). These experiments compared the compaction caused by vehicles of various weights. The plot area was completely covered by traffic with none of the area left untrafficked. Results typically showed differences in cone index and bulk density.

The axle load concept, while useful, does not offer any alternatives to reduce soil compaction other than reducing vehicle weight. Recent research results reported by Raper et al. (1993a), Bailey et al. (1993), and Raper et al. (1993b) showed that significant differences in soil-tire interface stresses, soil stresses, and tractive parameters occurred with changes of inflation pressure using the same axle load and radial tires. One reason that the axle load concept may not explain these differences is that the study upon which it is based (Taylor et al., 1980) used bias-ply tires. For larger tractors with substantial axle load (tractors over I00-hp), bias-ply tires are rarely sold in 1994. When the inflation pressure of a radial tire is increased, the footprint becomes shorter thus concentrating the load in a much smaller area (Raper et al., 1993b).

The objectives of this research effort are to:

1) examine peak values of soil-tire interface stress for dynamic load and inflation pressure effects,
2) use these soil-tire interface stresses to load a finite element model, and
3) examine the depth and degree of predicted soil stresses and compare to measured values.

MATERIALS AND METHODS

An experiment was conducted in the soil bins at the USDA-ARS National Soil Dynamics Laboratory to determine the effects of inflation pressure on soil-tire interface stresses, soil stresses, soil compaction, and tire performance. This experiment was conducted in a soil bin containing Norfolk sandy loam soil. Two soil conditions were used for this experiment. The first soil condition was created by using a rotary tiller to till the soil down to a depth of 60 cm and is called a uniformly loose soil condition. The second soil condition was created by rotary tilling the soil and then creating a hardpan layer with a moldboard plow and a heavily loaded rigid wheel. This soil condition is called the hardpan condition. The depth of the hardpan in the Norfolk sandy loam soil was 41 cm.

The tractor tire used in the experiment was a Goodyear[1] 18.4 R38 Dyna Torque Radial (2 star) R-l agricultural tractor tire. The Traction Research Vehicle was used to conduct the experiment. This machine is capable of operating and controlling a single tire for use in the soil bins, as described by Burt et al. (1980) and Lyne et al. (1983).

Load levels of 13.1 kN and 25.3 kN were used to load the radial-ply tire at inflation pressures of 41 kPa and 124 kPa. The notation used throughout this paper is that the first set of numbers in boldcase defines the dynamic load and the second set of

[1]The use of tradenames or company names does not imply endorsement by USDA-ARS or Auburn University.

numbers indicates the inflation pressure. The lower pair **(13.1 - 41)** and upper pair **(25.3 - 124)** of dynamic loads and inflation pressures were recommended values by the tire manufacturers. The other pairs of loads and inflation pressures are an overloaded **(25.3 - 41)** and an underloaded **(13.1 - 124)** case. These four combinations form a 2x2 factorial experiment. Four replications of each load condition were run with a constant level of slip of 10% used for all tests.

Soil stress state transducers (SST's) (Nichols et al., 1987) were buried in the center of the path of the tire. These transducers measured the pressure in six directions and provided values that allowed the calculations of octahedral normal and shearing stresses. These transducers were buried at the depth of the hardpan and halfway between the hardpan and the surface. The transducers were buried at an equivalent hardpan depth in the soil without a hardpan. Values resulting from the SST's were compared against the finite element predicted values of soil stress at similar depths. The full results of the SST measurements were reported in Bailey et al. (1993).

Seven soil-tire interface stress transducers were mounted both on the lug of the tire and in the undertread area (Figure 1). The full results of the soil-tire interface stress measurements were reported by Raper et al. (1993a) and Raper et al. (1993b). Data obtained from the soil-tire interface stress transducers were used to apply loads to the finite element model. An example set of soil-tire interface stresses is given in Figure 2. The peak values occurring on the surface of the lug as the tire passes through its entire rotation are taken to be the values that would most directly influence soil compaction. These peak values would occur every time a lug comes into contact with the soil.

The finite element program used to model the soil response to tire loading is the result of research conducted to determine the distribution of soil stresses and strains beneath loads placed on the soil surface (Raper et al., 1994). A plane strain model was used that assumed that the loading under the tire is constant and continuous in the plane perpendicular to the paper (Figure 3).

The soil constitutive relationship used to model the behavior of agricultural soil is based on research by Bailey and Johnson (1989).

$$\bar{\epsilon}_v = (A + B\sigma_{oct})(1 - e^{(-C\sigma_{oct})}) + D\left(\frac{\tau_{oct}}{\sigma_{oct}}\right) \qquad \textbf{(1)}$$

where $\bar{\epsilon}_y$ = natural volumetric strain, In (volume / original volume)
σ_{oct} = octahedral normal stress, kPa
τ_{oct} = octahedral shearing stress, kPa
A, B, C, D = compactibility coefficients

The octahedral stresses are defined according to the following equations.

$$\sigma_{oct} = (\sigma_1+\sigma_2+\sigma_3)/3 \quad \textbf{(2)}$$

$$_{oct} = [\sqrt{(\sigma_1-\sigma_2)^2+(\sigma_2-\sigma_3)^2+(\sigma_3-\sigma_1)^2}\,]/3 \quad \textbf{(3)}$$

where σ_1, σ_2, σ_3 = the principal stresses.

Limitations were placed on the octahedral shearing stress in Equation 1 to indicate maximum density at plastic flow.

$$\tau_{oct_y} = K\sigma_{oct} \quad \textbf{(4)}$$

where τ_{octy} = ultimate shearing stress at maximum density
K = a coefficient representing soil plastic flow yield.

The above models were based on triaxial data obtained up to maximum applied stress values of 500 kPa.

Predictions of the linear-elastic parameters, Young's modulus **(E),** and Poisson's ratio (v) were made at each load step based on the predicted stress values for each element in the model (Raper et al., 1994). These values were used to compute the next load step's values of stress and strain which were then used to compute the following load step's linear-elastic parameters. This stepwise approach was used for 20 load steps which was sufficient to model the non-linear behavior of agricultural soil.

RESULTS AND DISCUSSION

An average peak soil-tire interface stress for each transducer location was found over the four replications for each dynamic load-inflation pressure combination in each soil condition. The peak soil-tire interface stresses measured on each transducer across the lug of the tire showed both dynamic load and inflation pressure effects in the hardpan soil condition and in the uniformly loose soil condition (Figures 4 and 5). In the hardpan condition (Figure 4), inflation pressure effects were greatest near the center of the tire. At this transducer location, both high inflation pressure treatments (124 kPa) were significantly greater than both low inflation pressure treatments (41 kPa). Away from the tire centerline, differences between dynamic loads at the same inflation pressure were noticeable. At the two middle soil-tire interface stress transducers on the

lug, differences between the **13.1 - 124** treatment and the **25.3 - 41** treatment were not statistically significant. Only at the outer edge of the tire were the dynamic load effects of both high load treatments (25.3 kN) greater than those of both low dynamic loads (13.1 kN).

For the uniformly loose soil condition (Figure 5), many of the same trends were seen for both dynamic load and inflation pressure as in Figure 4. For the tire centerline, statistical differences were only seen for the two levels of inflation pressure (41 kPa and 124 kPa). For the two middle transducers, a dynamic load effect was especially evident for the **25.3 - 124** treatment. At the transducer location next to the tire centerline, the **13.1 - 124** load treatment was also statistically greater than the **13.1 - 41** and the **25.3 - 41** load treatments. At the next location away from the tire centerline, the **25.3 - 124** load treatment was statistically greater than any of the other three load treatments that were essentially equal. Again at the tire edge, the dynamic load effect was statistically significant with clear distinctions being seen between the low (13.1 kN) and the high (25.3 kN) dynamic loads.

Figures 4 and 5 can be used as evidence to show that either dynamic load or axle load effects do not independently control the maximum amount of soil-tire interface stress over the surface of the lug. Only near the outer edge of the tire is the effect of dynamic load significant. These same two figures show that inflation pressure does not totally control the maximum amount of soil-tire interface stress over the surface of the lug. Only at the center of the tire is the effect of inflation pressure statistically significant. Both parameters, dynamic load and inflation pressure, must be considered in evaluating the causes of high stress at the soil-tire interface.

The use of peak soil-tire interface stresses from Figure 5 for the uniformly loose soil condition as input loads for the finite element model produces reasonable stress distributions within the soil. Figures 6, 7, 8, and 9 show the finite-element predicted octahedral normal stress iso-stress lines for the treatment conditions **13.1 - 41, 13.1 - 124, 25.3 - 41,** and **25.3 - 124,** respectively. One item that is evident in each of the four graphs is that the location of the peak octahedral normal stress is not beneath the center of the tire. In each case, it is located beneath the outer edge of the tire where the surface loading was typically greatest.

Comparisons of Figures 6 and 7 for the **13.1 - 41** and **13.1 - 124** load treatments shows that inflation pressure alone caused differences in the predicted octahedral normal stress iso-stress lines. In particular for the **13.1 - 124** load condition, note the increased levels of stress near the surface under the edge of the tire and the deeper penetration of the 40 and 50 kPa iso-stress lines, These graphs suggest that inflation pressure can affect compaction much deeper than the soil surface.

Another comparison that tends to show the interaction between dynamic load and inflation pressure is seen when examining Figures 7 and 8. These figures differ in dynamic load and inflation pressure. These figures are very similar with the higher inflation pressure in Figure 7 creating a similar soil stress condition to Figure 8 that has a larger dynamic load. Although the tire for the **25.3 - 41** load condition is operating at a lower inflation pressure than the manufacturer recommends, the predicted stress

distribution suggests that it is possible to compensate for increased loads to some extent by decreasing inflation pressure and increasing the tire footprint.

Comparing the values of finite-element predicted stress to those obtained from the SST shows that the model accurately predicted the octahedral stress levels in most cases (Table 1). The cells that are shaded indicate stress predictions that are outside a 95% confidence interval. Only for the load condition **25.3 - 41** does the model fail to predict the octahedral normal and shearing stresses at both depths accurately. Even for this load condition, however, the 95% confidence intervals are narrowly missed by the finite element predictions. This is probably due to the nonuniformity of the loading occurring across the width of the tire (Figure 5). The peak soil-tire interface stresses for the other loads occurred more uniformly across the tire.

The finite element model predictions are useful for several reasons. They tend to indicate differences in stress levels caused by different dynamic loads and inflation pressures and their complex interactions. These predictions also demonstrate that the areas of maximum stress occurred not under the center of the tire, but under the outer edge of the tire. Future experiments should obtain stress values in this area to help validate the model.

CONCLUSIONS

(1) Soil-tire interface stress on a tire lug was found to be affected by dynamic load at the outer edge of the tire. Inflation pressure effects were found at the center of the tire. In between these two locations, dynamic load - inflation pressure interactions were found. These results indicate that neither dynamic load nor inflation pressure is totally responsible for the peak values of soil-tire interface stresses measured across the tire lug.

(2) The predicted iso-stress lines for the different dynamic load - inflation pressure combinations showed that similar soil stress patterns can develop for tires with different inflation pressures and different dynamic loads. The interaction of these two tire operational parameters requires that both variables be optimized to limit soil compaction.

(3) The octahedral normal and shear stress values measured by the SST were mostly predicted within a 95% confidence interval by the finite element model.

REFERENCES

Bailey, A.C. and C.E. Johnson. 1989. A soil compaction model for cylindrical stress states. Trans. ASAE 32(3):822-825.

Bailey, A.C., R.L. Raper, T.R. Way, E.C. Burt, and C.E. Johnson. Soil stresses under tractor tires at various inflation pressures. Proceedings of the 11th Annual Conference of the International Society for Terrain-Vehicle Systems, Incline Village, CA. Sept 27-30, 1993.

Boussinesq., J. 1885. Application des Potentials a l'Etude de l'Equilibre et du Mouvement des Solides Elastiques. (Application of Potentials in the Study of the Equilibrium and the Movement of Elastic Solids). Gauthier-Villais, Paris, France, 30 pp. (in French).

Burt, E.C., C.A. Reaves, A.C. Bailey, and W.D. Pickering. 1980. A machine for testing tractor tires in soil bins. Trans. of ASAE 23(3):546-547, 552.

Chi, L. and R.L. Kushwaha. 1989. Finite element analysis of soil forces on two shapes of tillage tool. Am. Soc. Agric. Eng., St. Joseph, MI., USA., ASAE Pap. 89-1103.

Chi, L., S. Tessier, and C. Lague. 1993. Finite element prediction of soil compaction induced by various running gears. Trans. of ASAE 36(3):629-636.

Duncan, J.M. and C.Y. Chang. 1970. Nonlinear analysis of stress and strain in soils. J. Soil Mech. Foun. Div., Proc. Am. Soc. Civil Eng., 96:1629-1653.

Frohlich, O.K. 1934. Druckverteilung im Baugrunde. (Pressure distribution in foundation soils). Springer, Wien, Austria, 178 pp. (in German).

Hakansson, I. 1994. Subsoil compaction by high axle load traffic. Soil and Tillage Research 29(2 and 3) Special Issue.

Lyne, P.W.L., E.C. Burt, and J.D. Jarrell. 1983. Computer control for the National Tillage Machinery Laboratory single-wheel tester. ASAE Paper No. 83-1555, ASAE, St. Joseph, Ml 49085.

Nichols, T.A., A.C. Bailey, C.E. Johnson, and R.D. Grisso. 1987. A stress state transducer for soil. Trans. ASAE, 30(5):1237-1241.

Perumpral, J.V., J.B. Liljedahl, and W.H. Perloff. 1971. The finite element method for predicting stress distribution and soil deformation under tractive devices. Trans. ASAE 14: 1184-1188.

Pollock, D. Jr., J.V. Perumpral, and T. Kuppusamy. 1986. Finite element analysis of multipass effects of vehicles on soil compaction. Trans. ASAE 29(1):45-50.

Raper, R.L. and D.C. Erbach. 1990. Prediction of soil stresses using the finite element method. Trans. ASAE 33(3):725-730.

Raper, R.L., A.C. Bailey, E.C. Burt, T.R. Way, and P. Liberati. 1993a. Inflation pressure effects on soil-tire interface stresses. Proceedings of the 11th Annual Conference of the International Society for Terrain-Vehicle Systems, Incline Village, CA. Sept 27-30.

Raper, R.L., A.C. Bailey, E.C. Burt, T.R. Way, and P. Liberati. 1993b. Inflation pressure and dynamic load effects on soil deformation and soil-tire interface stresses. ASAE Paper No. 931517. ASAE, St. Joseph, MI.

Raper, R.L., C.E. Johnson, A.C. Bailey, E.C. Burt, and W.A. Block. 1992. Using the finite element method to predict soil stresses beneath a rigid wheel. Proceedings of the 4th North American Regional Meeting of ISTVS, Sacramento, CA, March 25-27, pp. 144-151.

Raper, R.L., C.E. Johnson. and A.C. Bailey. 1994. Coupling normal and shearing stresses to use in finite element prediction of soil stresses -An application of the NSDL-AU soil compaction model. Trans. ASAE (IN PRESS).

Taylor, J.H., E.C. Burt, and A.C. Bailey. 1980. Effect of total load on subsurface soil compaction. Trans. ASAE 23(3):568-570.

TABLE 1. Final depths of SST's, peak octahedral normal stresses, and octahedral shear stresses at peak octahedral normal stresses of the SST's for the Norfolk sandy loam soil in the uniformly loose soil condition. The 95% confidence intervals are also shown for the stresses. The predicted values which failed to be inside a 95% CI are shown in the shaded cells.

TREATMENT	FINAL SST DEPTH	PEAK σ_{OCT}		τ_{OCT} at PEAK σ_{OCT}	
		MEASURED	PREDICTED	MEASURED	PREDICTED
	cm	kPa	kPa	kPa	kPa
13.1-41	29.6	43.6 ± 7.5	38.2	51.9 ± 27.9	28.9
13.1-41	37.5	32.4 ± 5.1	37.5	32.3 ± 4.4	28.9
13.1-124	30.1	49.1 ± 10.6	46.5	54.5 ± 24.7	35.1
13.1-124	37.8	43.0 ± 14.1	47.4	54.7 ± 31.1	34.7
25.3-41	31.4	52.5 ± 9.3	43.0	55.9 ± 22.3	32.2
25.3-41	38.3	51.1 ± 8.0	42.5	55.4 ± 15.6	33.1
25.3-124	32.3	81.7 ± 11.6	62.7	89.2 ± 27.3	47.4
25.3-124	39.1	56.7 ± 12.7	61.7	56.4 ± 23.0	46.4

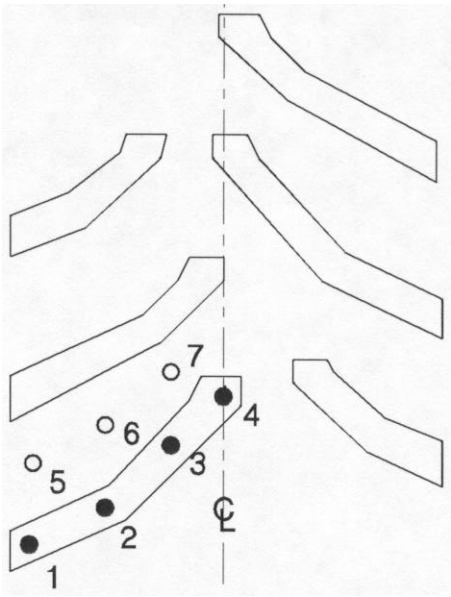

Figure 1. Locations of soil-tire interface stress transducers on an 18.4 R38 radial tractor tire.

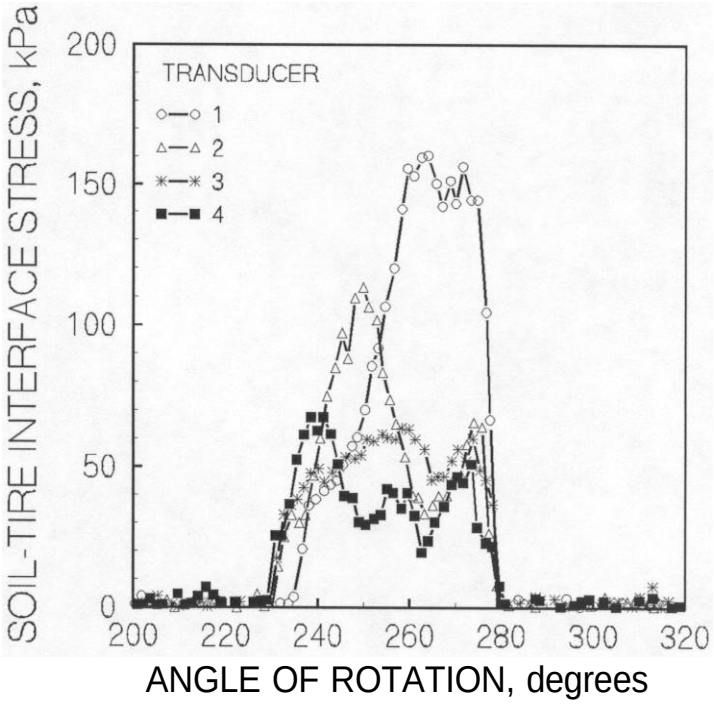

Figure 2. Soil-tire interface stresses across the lug of the tire for first replication of the uniformly loose soil condition using the **13.1- 41** load condition.

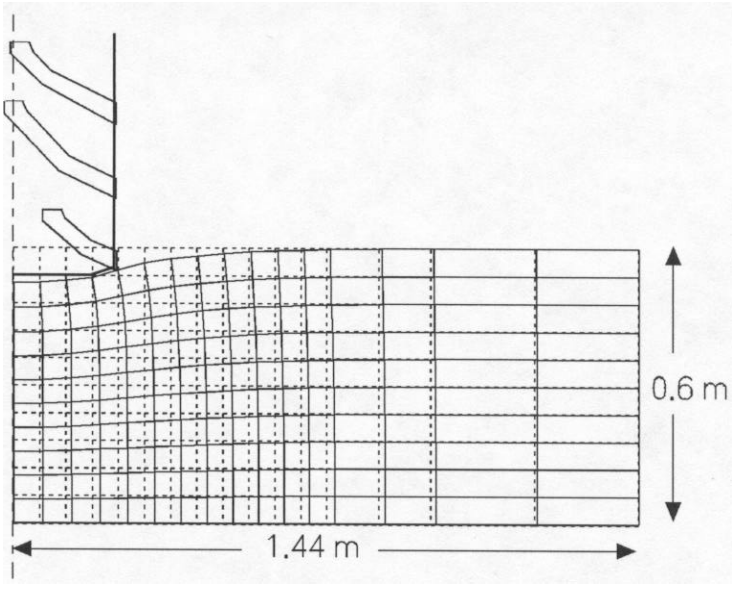

Figure 3. Original and deformed mesh for the **13.1 - 124** load condition.

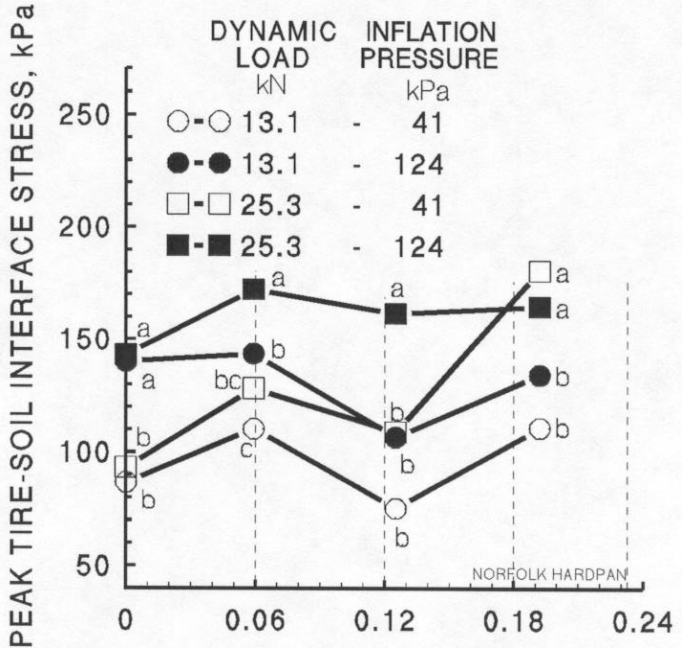

Figure 4. Peak soil-tire interface stresses measured across the tire lugs in the Norfolk sandy loam soil when it was in a hardpan condition. The dashed lines indicate the location of the nodes in the finite element model.

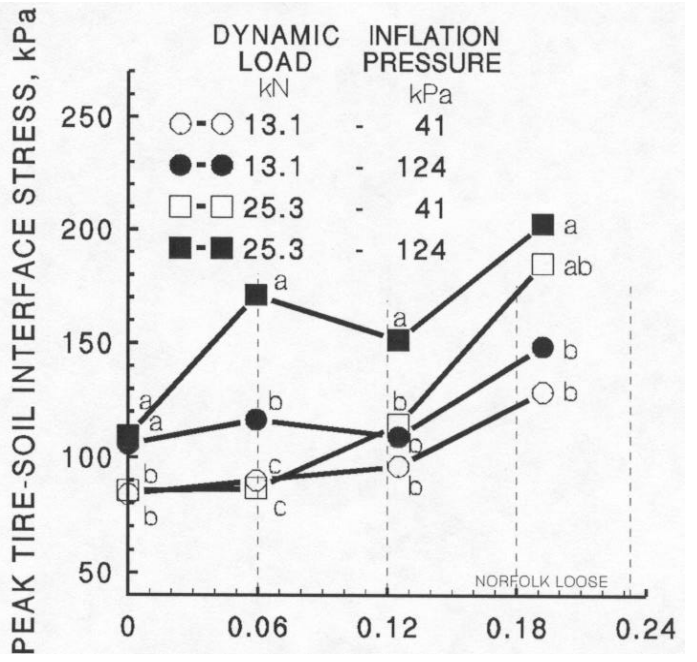

Figure 5. Peak soil-tire interface stresses measured across the tire lugs in the Norfolk sandy loam soil when it was in a uniformly loose condition. The dashed lines indicate the location of the nodes in the finite element model.

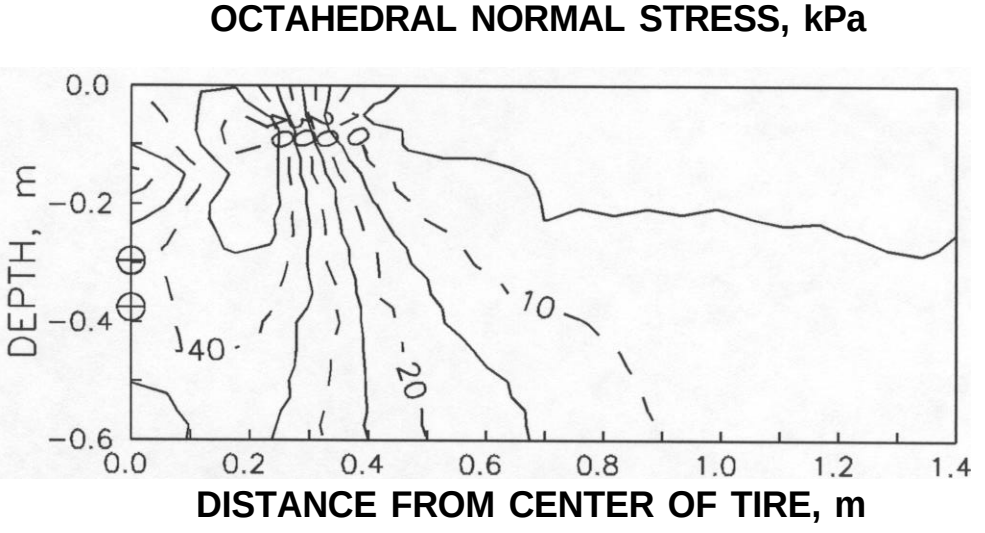

Figure 6. Finite element predicted octahedral normal stress iso-lines for the **13.1 - 41** load condition in the Norfolk sandy loam soil in the uniformly loose soil condition. The circles on the left y axis denote the final location of the SST's.

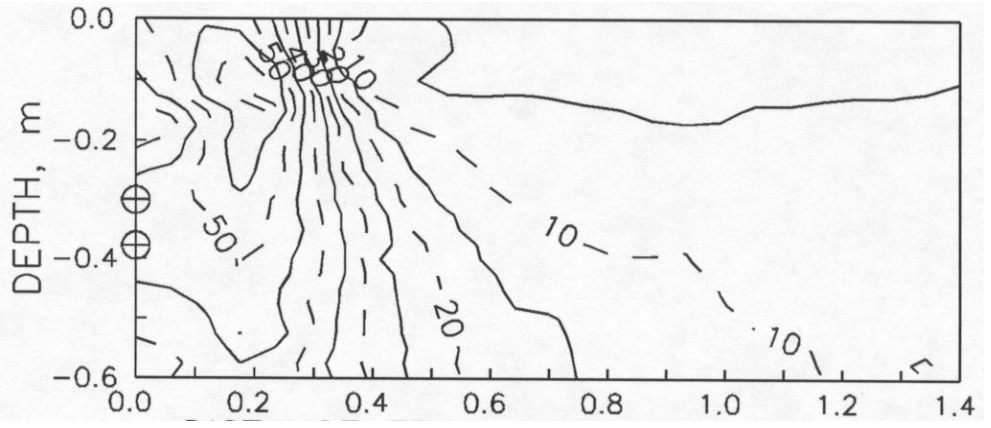

Figure 7. Finite element predicted octahedral normal stress isolines for the **13.1 - 124** load condition in the Norfolk sandy loam soil in the uniformly loose soil condition. The circles on the left y axis denote the final location of the SST's,

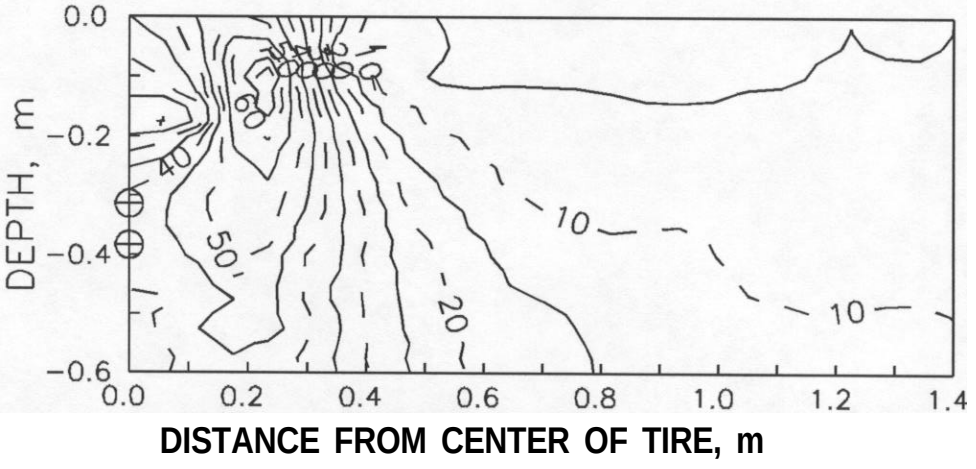

Figure 8. Finite element predicted octahedral normal stress isolines for the **25.3 - 41** load condition in the Norfolk sandy loam soil in the uniformly loose soil condition. The circles on the left y axis denote the final location of the SST's,

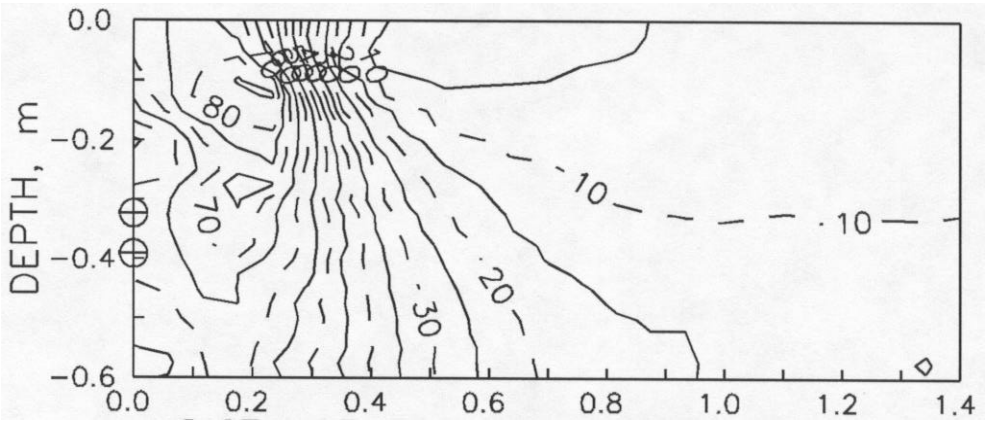

Figure 9. Finite element predicted octahedral normal stress isolines for the **25.3 - 124** load condition in the Norfolk sandy loam soil in the uniformly loose soil condition. The circles on the lefty axis denote the final location of the SST's.